Received: 3 April 2019 | Revised: 24 June 2019 | Accepted: 22 August 2019

DOI: 10.1111/clr.13531

ORIGINAL RESEARCH

CLINICAL ORAL IMPLANTS RESEARCH WILEY

# Can implants move in bone? A longitudinal in vivo micro-CT analysis of implants under constant forces in rat vertebrae

Kathrin Becker[1,2] | Frank Schwarz[2] | Nicole Jasmin Rauch[1] | Silava Khalaph[1] | Ilja Mihatovic[3] | Dieter Drescher[1]

[1]Department of Orthodontics, Universitätsklinikum Düsseldorf, Düsseldorf, Germany

[2]Department of Oral Surgery and Implantology, Carolinum, Goethe University, Frankfurt, Germany

[3]Department of Oral Surgery, Universitätsklinikum Düsseldorf, Düsseldorf, Germany

**Correspondence**
Kathrin Becker, Department of Orthodontics, Westdeutsche Kieferklinik, Heinrich-Heine-University, D-40225 Düsseldorf, Germany.
Email: Kathrin.Becker@med.uni-duesseldorf.de

**Funding information**
The study was supported by the Deutsche Forschungsgemeinschaft (DFG, Bonn, Germany, project number: 318755096, reference number: BE 5350/1-1).

## Abstract

**Objectives:** Whereas stationary stability of implants has been postulated for decades, recent studies suggested a phenomenon termed implant migration. This describes a change in position of implants as a reaction to applied forces. The present study aims at employing image registration of in vivo micro-CT scans from different time points and to assess (a) if migration of continuously loaded implants is possible and (b) migration correlates with the force magnitude.

**Material and methods:** Two customized machined implants were placed in the dorsal portion of caudal vertebrae in $n$ = 61 rats and exposed to standardized forces (0.5 N, 1.0 N, and 1.5 N) applied through a flat nickel–titanium contraction spring, or no forces (control). Micro-CT scans were performed at 0, 1, 2, 4, 6, and 8 weeks after surgery. The baseline image was registered with the forthcoming scans. Implant migration was measured as the Euclidean distance between implant tips. Bone remodeling was assessed between the baseline and the forthcoming scans.

**Results:** The findings confirmed a positional change of the implants at 2 and 8 weeks of healing, and a linear association between applied force and velocity of movement (anterior implant: $\chi^2$ = 12.12, $df$ = 3, and $p$ = .007 and posterior implant: $\chi^2$ = 20.35, $df$ = 3, and $p$ < .001). Bone apposition was observed around the implants and accompanied by formation of load-bearing trabeculae and a general cortical thickening close and also distant to the implants.

**Conclusion:** The present analysis confirmed that implants can migrate in bone. The applied forces seemed to stimulate bone thickening, which could explain why implants migrate without affecting stability.

KEYWORDS

bone-screw, implant movement, implant stability, in vivo micro-CT, orthodontic mini-implant

## 1 | INTRODUCTION

Since the introduction of palatal implants and orthodontic mini-screws in the mid-1990s (Kanomi, 1997; Melsen & Costa, 2000; Park, Bae, Kyung, & Sung, 2001; Wehrbein, Glatzmaier, Mundwiller, & Diedrich, 1996; Wehrbein, Merz, Diedrich, & Glatzmaier, 1996), skeletal anchorage is increasingly employed to enhance orthodontic anchorage. In recent years, therapeutic advantage could be

demonstrated for several indications including en-masse retraction of the front (Becker, Pliska, et al., 2018), skeletally anchored protraction of the maxilla in early class III treatments (Meyns, Brasil, Mazzi-Chaves, Politis, & Jacobs, 2018; Rodriguez de Guzman-Barrera et al., 2017), and for the mesialization and distalization of molars (Becker, Wilmes, Grandjean, Vasudavan, & Drescher, 2018; Wilmes, Katyal, & Drescher, 2014).

As temporary anchorage devices are commonly removed after usage, requirements differ from dental implants. Commonly, they are composed of titanium alloys to improve mechanical stability, have a reduced diameter of 1.2–2.3 mm and a smooth surface to ease removal. They are loaded with constant directed forces of 50 g–400 g either immediately or after a healing period which varies considerable in literature (Reynders, Ronchi, & Bipat, 2009). Despite high success rates (Papageorgiou, Zogakis, & Papadopoulos, 2012), recent clinical studies observed a phenomenon termed "implant migration" describing a displacement of an implant while maintaining stability (Nienkemper, Handschel, & Drescher, 2014). This observation is in contradiction with the belief that implants remain stationary in bone, and that migration would be associated with inflammation and loss of stability. The underlying biological principle has not yet been discovered.

Until today, it is neither known if this phenomenon really exists nor if it is associated with the magnitude of applied force. Some authors suggested that it may be a consequence to the trauma of implant insertion, or even a result of the elastic properties of bone and would thus occur only in the initial healing phase (Alves, Baratieri, & Nojima, 2011), whereas two studies reported significant displacement during the entire treatment period (Liou, Pai, & Lin, 2004; Wang & Liou, 2008).

With the advent of in vivo micro-computed tomography (μCT), high-resolution scans can be obtained at different time points from the same animal (Dall'Ara et al., 2016; Li et al., 2015; Zhou et al., 2018). While metal artefacts can impede the analysis of the bone-to-implant interface and the peri-implant bone tissue, μCT is appropriate to assess positional changes of dense materials including mini-implants (Becker, Stauber, Schwarz, & Beissbarth, 2015).

Hence, the present study aimed at employing in vivo μCT in rats to assess (a) if implants can move in bone while remaining osseointegrated and (b) to assess association between positional changes and the magnitude of applied force.

## 2 | MATERIAL AND METHODS

### 2.1 | Animals

A total of $n$ = 61 female albino rats of the Wistar strain (mean weight 263 ± 20 g and age 15.4 ± 3.9 weeks) were used in the study (further, four animals died preoperatively during narcosis, five animals died during the post-operative in vivo μCT scan, and one rat died during the in vivo μCT scan at 4 weeks after surgery). During all experimental days, the animals were fed with standard laboratory food pellets and water ad libitum. The study protocol was approved by the appropriate local authority (Landesamt für Natur und Verbraucherschutz) and conformed with the ARRIVE Guidelines. The experimental part of the study started after an adaption period of 1 week.

### 2.2 | Study design

The animals were allocated to the following groups: (a) Loading with high force (1.5 N), (b) loading with medium force (1.0 N), (c) loading with low forces (0.5 N), and (d) no loading (0 N, control). The loading was applied using a flat customized nickel–titanium spring (RISystem AG) mounted to two customized mini-implants (RISystem AG) (Figure 1), which were inserted into the dorsal portion of a caudal rat vertebrae. 50% of the animals were killed after 2 weeks of healing, and the remaining animals were killed after 8 weeks (original assignment: $n$ = 16 animals per group).

#### 2.2.1 | Customized nickel–titanium spring

The flat nickel–titanium contraction springs were drafted by two authors of the study (K.B. and D.D.) to facilitate subcutaneous loading of the implants. They were fabricated by RISystem (RISystem AG) out of nickel–titanium sheets (Johnson Matthey) with suitable properties (Nickel: 55.8%, Elongation: 11.5%, and $A_f$: 7.2°C). To maintain super-elastic properties following cutting, waterjet machining was employed (Kong, Axinte, & Voice, 2011). Differential scanning calorimetry (DSC) was performed for one specimen after fabrication of the spring to ensure that no detrimental effects, that is, change of transformation temperature austenite finish temperature ($A_f$), occurred during cutting (Figure 2a). Three thicknesses were used (0.15 mm, 0.2 mm, and 0.25 mm) to achieve super-elastic behavior in the desired force ranges (i.e., 0.5 N, 1.0 N, and 1.5 N). For each spring, the super-elastic range

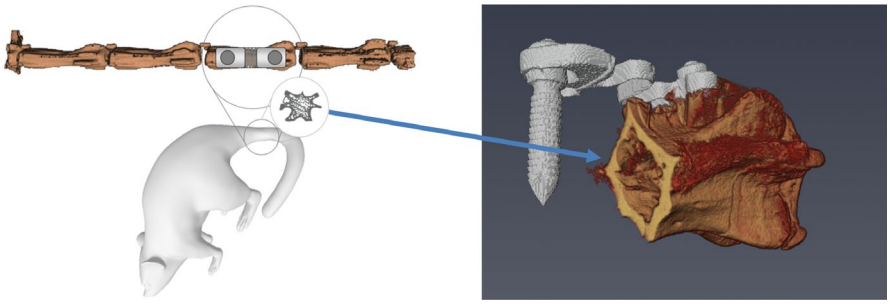

**FIGURE 1** Visualization of the animal model. Two implants (TAV, 0.8 × 3.0 mm, RA 0.8 μm) were inserted into a tail vertebra of a rat and connected by a flat nickel–titanium spring spanned such that it was in its super-elastic range and applied forces of (1.5 N, 1.0 N, or 0.5 N). In the control group, the spring was inserted passively

at 28°C (tail temperature) was assessed through force deflection diagrams coming from contraction tests conducted with a precision robot (Stäubli RX 60, Stäubli Tec-Systems) (Figure 2b-d).

### 2.2.2 | Customized mini-implants

The mini-implants (Ti-6Al-4V, 0.8 × 3.0 mm, Ra 0.8) were designed and manufactured by RISystem (RISystem AG) and had a snap-in hole for the spring at the implant head. Scanning electron microscopy was performed to assess surface topography of the mini-implants (Figure 3a-d). The screw-in arms at the top of the implants were removed after placement by stressing the breaking point. The optimal distance of the mini-implants was selected according to the respective super-elastic range in the force deflection diagram.

## 2.3 | Anesthesia protocol

A standardized anesthesia protocol was followed during each surgical intervention. The animals were anesthetized by intraperitoneal injection of 100 mg/kg ketamine (Ketanest®, Pfizer Pharma GmbH) and 5 mg/kg xylazine (Rompun®, Bayer HealthCare). For post-operative analgesia, 0.01 mg/L buprenorphine at a dose of 0.03 mg/kg (days 1–3, subcutaneous application three times per day) was applied.

## 2.4 | Surgical procedure

All surgeries were performed by two experienced clinicians (K. B. and I. M.). The tails were disinfected with polyvidone iodine (Betaisodona®, Mundipharma). A dorsal incision was made below the sacrum at the hairless tail. Subsequently, the skin, the dorsal segmental muscles, and the caudal nerves were carefully prepared and retracted, and the vertebrae were exposed. The respective implant position was determined according to their desired distance (super-elastic range of the spring). Pre-drilling was performed using customized drill-bits (RISystem AG). The implants were inserted through the holes in the spring plate such that the snap-in holes were oriented to the intervertebral disks. After implant placement, it was ensured that the spring snapped into the designated holes. Finally, the drew-in arms were removed (Figure 4).

After insertion of the apparatus, the inner and outer skin were closed separately using resorbable 4.0 vicryl polyglycol suture material (Resorba®). Post-operatively, the weight of each animal, the overall well-being, and the wound state were recorded once per day in the first week and once per week thereafter.

Post-operatively, the animals had to wear an in-house fabricated toby collar for 2 weeks (constructed by N. R.). Additionally, they were housed in single cages during the entire experiment to avoid manipulation of the wounds.

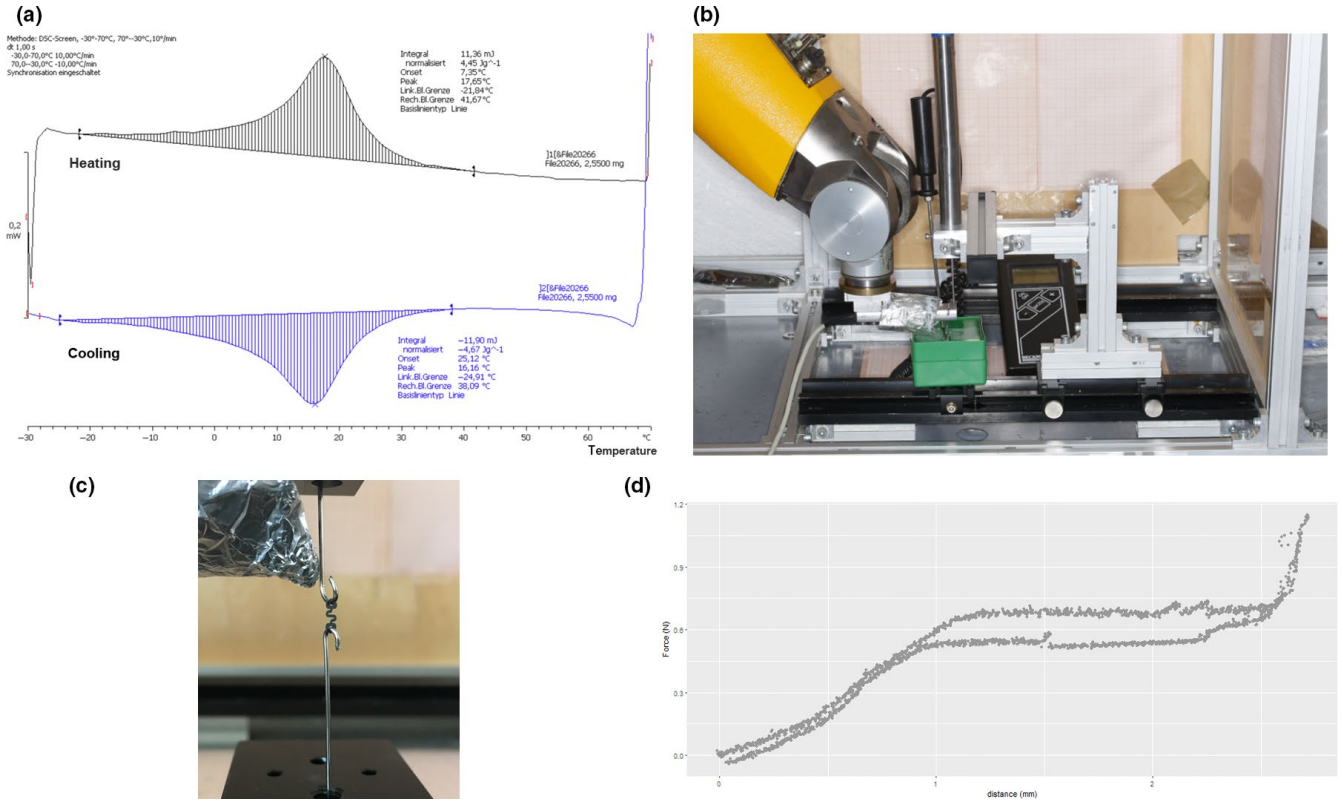


**FIGURE 2** (a) DSC analysis of a nickel–titanium spring after fabrication. Phase transformation during heating ranged from −20°C to 42°C (peak 17.65°C). During cooling, it ranged from 38°C to −22°C (peak 16°C). (b, c) Photographs of the robot that was used to perform biomechanical evaluation of the springs. (d) Example of a force–distance diagram used to assess the super-elastic range

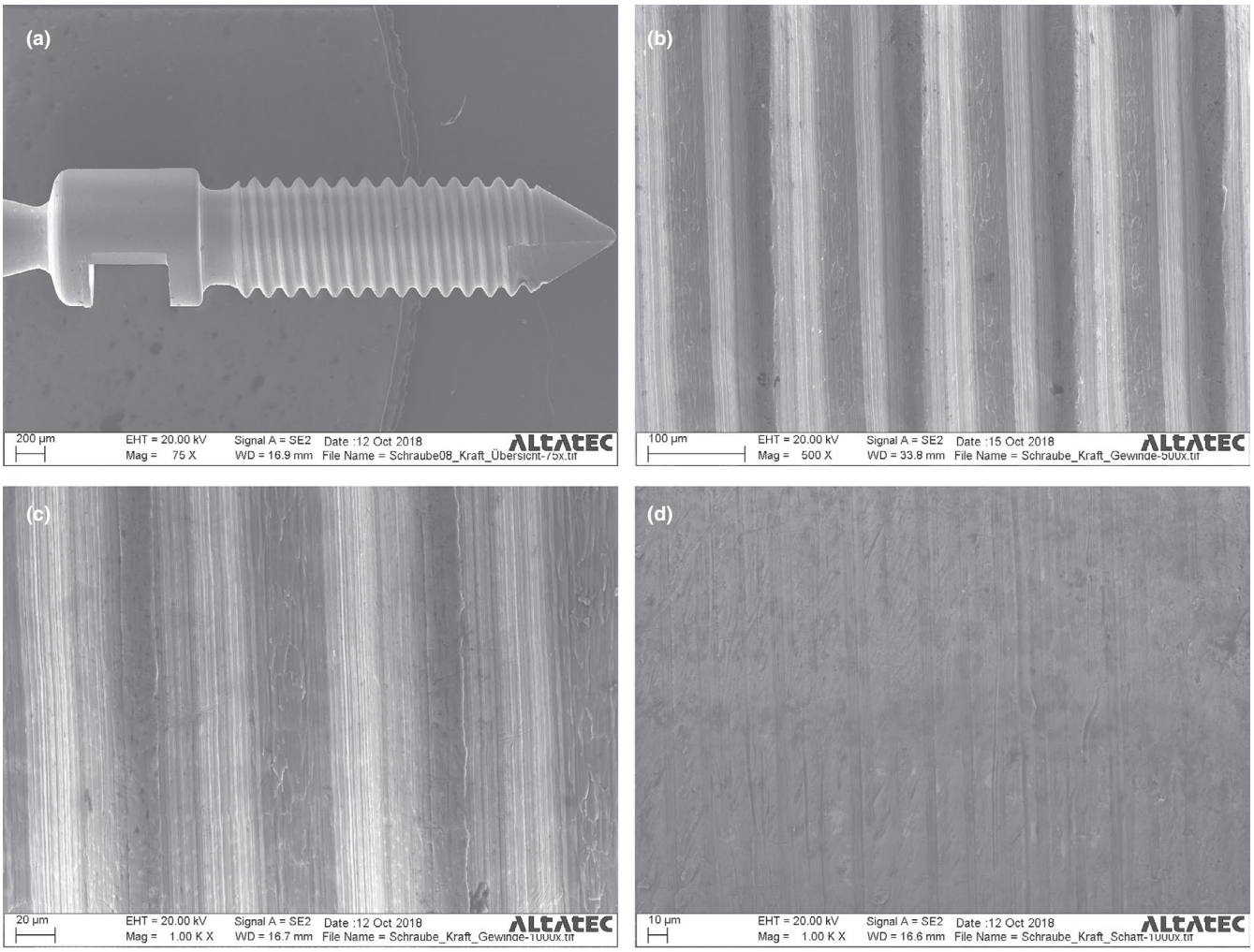


**FIGURE 3** Scanning electron microscopy of the mini-implants: (a) an overview, (b) 500× magnification, (c) 1000× magnification (implant thread), and (d) 1000× magnification (implant neck)

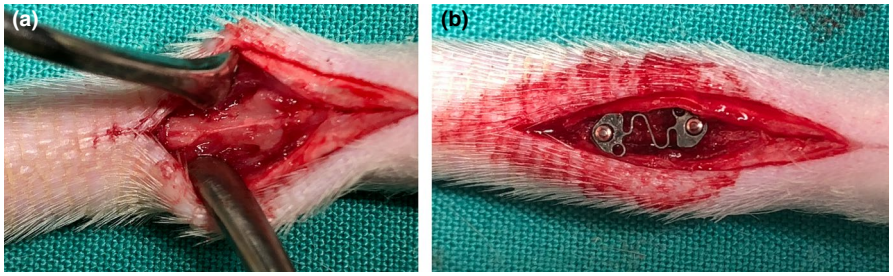


**FIGURE 4** Photograph of the surgical procedure, that is, preparation of the vertebra (a) and mini-implant insertion and placement of the spring (b)

## 2.5 | In vivo micro-computed tomography

To assess the dynamics of implant movement, the animals were scanned with an in vivo µCT (Viva CT 80, Scanco Medical). µCT scans were performed directly after surgery (week 0), at week 1 and week 2, and a total of 32 animals were also scanned at 4, 6, and 8 weeks of healing. The scans were performed at 70 kVp, 114 µA, and 250 ms integration time and reconstructed to a nominal isotropic voxel size of 15.6 µm. The dual-stack mode was deactivated during image reconstruction. During all scans, the animals were anesthetized as described. Additionally, 0.07 ml Valium was applied to minimize tail movements while scanning. During the scans, the tail was fixed within a customized in-house fabricated rat tail holder made of methacrylate that was mounted within the µCT rat tail holder. Temperature and heart rate were monitored through specific sensors (Figure 5a-c). Warming of the animal was achieved through the inbuilt heating unit and additional warming pillows below the animal.

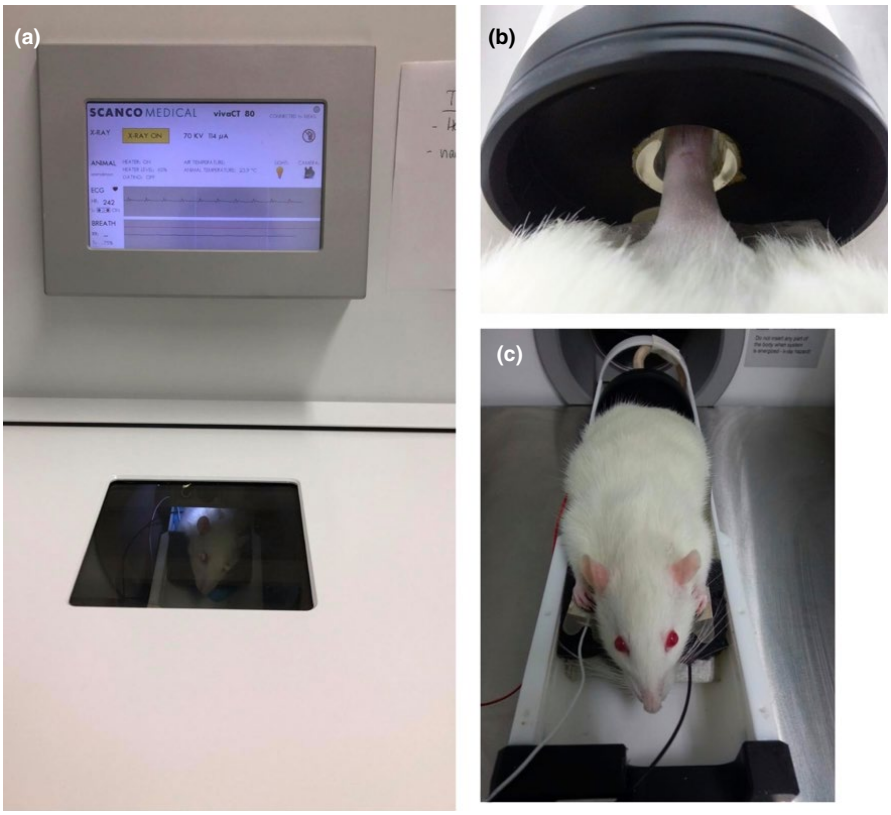


**FIGURE 5** Photographs of the in vivo scanning process. (a) Viva CT 80, (b) rat tail fixed in the general tail holder with transparent customized tail holder inside, (c) photograph of an animal connected to the temperature sensor and electrocardiogram

## 2.6 | Image processing

All scans were exported to the DICOM file format using ImageJ (National Institute of Health). Thereafter, image processing was performed using Amira software (Amira v6.5, Thermo Fisher Scientific).

### 2.6.1 | Feature extraction

Segmentation of the implants and the bone tissue was achieved through thresholding (upper and lower gray value limits for the implants and nickel–titanium spring: 99%–100% and bone tissue: 24%–76%).

### 2.6.2 | Image registration

The post-operative image served as baseline, and each forthcoming scan was registered with the previous one. For example, week 1 was registered with week 0, week 2 with week 1, and so on.

The image registration process itself included the following two steps:

1. *First guess* registration: The implants and the nickel–titanium springs were registered by minimizing the distance of their mean values and their principal components. This was achieved through subtraction of the respective mean values and rotation according to the differences in the first principal component. The obtained transformation matrix was then applied to the bone tissue of the moving image (forthcoming scan).
2. Fine registration: The bone tissues were rigidly registered by maximizing their normalized mutual information as described in (Studholme, Hill, & Hawkes, 1999). The transformation matrix was then applied to the respective implants and nickel–titanium spring.

The standardized image segmentation and registration procedures were executed by four blinded observers (S. K., V. T. S., M. H., P. J). Successful registration was validated visually through inspection by two of the blinded observers.

### 2.6.3 | Measurement of implant movement

To assess implant movement, linear distance measurements between the respective implant tips of two consecutive registered scans were performed by one blinded observer (S. K.). Calibration was achieved by repeating all distance measurements at the anterior implant after a period of 1 month. Additionally, whenever metal artefacts at the implant tip were noted, the same implant from another scan was superimposed to identify the implant tip accurately. When motion artefacts were noted, a discussion among all blinded observers was held (S. K., V. T. S., M. H., P. J.) to decide whether the artefacts could affect the distance measurements. In these cases, the scan was excluded. If applicable, the missing value was interpolated from the subsequent and previous measurements.

## 2.7 | Statistical analysis

The statistical analysis was performed using R (R Core Team, 2016). Error-plots showing the median and quartile ranges were generated

to visualize movement between the measurement time points for each group and implant position (anterior/posterior). Reliability of the repeated measurements was analyzed by estimating the intra-class correlation coefficient (ICC) and confidence intervals using the variance components from a one-way ANOVA. The R package *lme4* (Bates, Maechler, Bolker, & Walker, 2015) was used to perform a linear mixed effects analysis of the relationship between implant movement, applied force, and time point. As fixed effects, we entered the implant movement (μm) between subsequent measurements, the applied force (0 N, 0.5 N, 1.0 N, and 1.5 N) and the measurement interval (week 0–1, 1–2, 2–4, 4–6, and 6–8) into the model. As random effects, we had intercepts for animals. Visual inspection of residual plots did not reveal any obvious deviations from homoscedasticity or normality. *p*-Values were obtained by likelihood ratio tests of the full model with the effect in question against the model without the effect in question. Results were found significant at $p < .05$.

## 3 | RESULTS

The post-operative healing was considered as generally uneventful. No complications such as allergic reactions, abscesses, or infections were noted except for one animal, that repeatedly manipulated the wound. As the infection did not resolve and finally led to loss of one implant, this animal was excluded. The vertebra of two animals assigned to the high force group was too short for stretched contraction springs. Hence, these animals were assigned to the control group and received a passive spring. The health status, behavior, and feeding habits of each animal were not influenced by the experimental procedures.

### 3.1 | Image acquisition

In general, all in vivo scans were performed without complications. However, minor motion artifacts could not always be avoided. As they could affect linear measurements in the micrometer scale, scans from four animals were found affected and excluded upon discussion. One μCT scan terminated ahead of time and contained one implant only, so the value of the second implant had to be interpolated for the respective time point. Metal artifacts affected scans from four animals. Due to a sudden breakdown of the X-ray tube, no post-operative scans were possible in eight animals, but in vivo measurements could be resumed between week one and eight.

### 3.2 | Image registration

The two-step alignment procedure enabled successful image registration. It allowed to assess the displacement of the implants and the associated bone remodeling over time.

### 3.3 | Implant migration

Implant movement was measured in consecutive, registered scans. In six animals, the spring became loose during implant movement, so all subsequent scans had to be excluded because controlled force was no longer applied on the implants and manipulation from the spring could not be prohibited. Finally, the number of animals per group amounted to 17 (control), 16 (low force), 15 (medium force), and 12 (high force). Repetition of the distance measurements for the anterior implant revealed high reliability (ICC: 0.982, CI [alpha = 0.05]: 0.97–0.99).

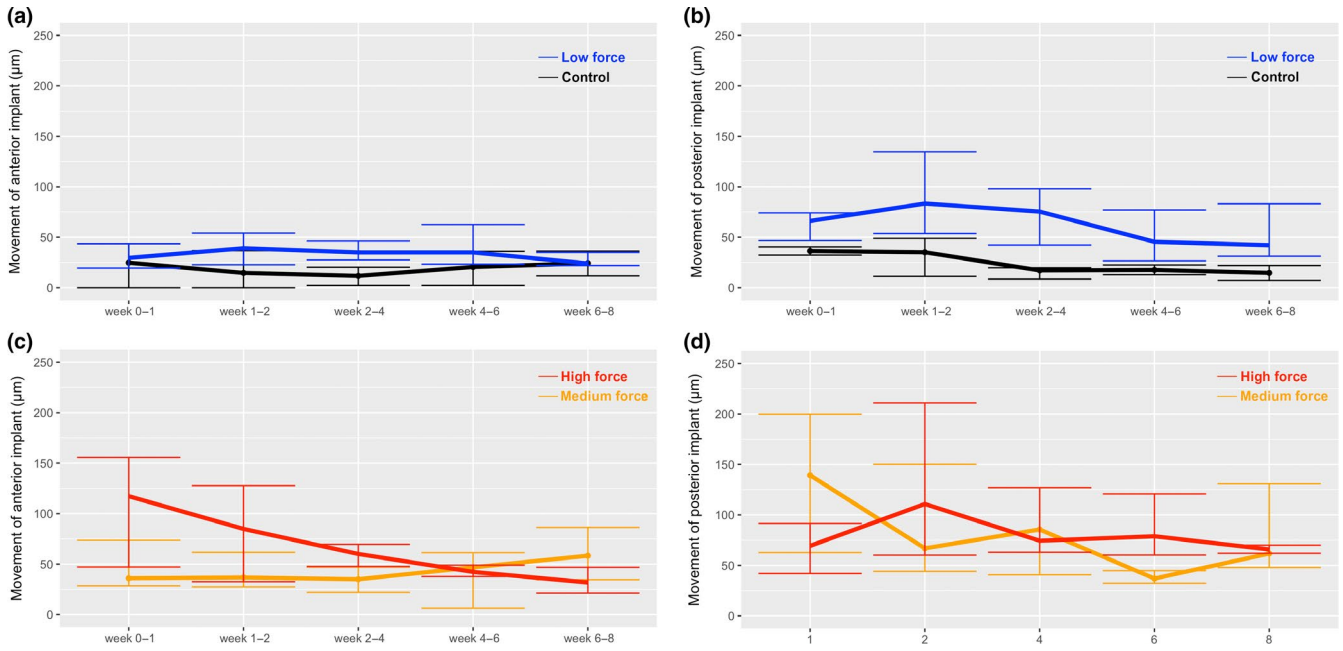


**FIGURE 6** Median and quartile ranges of the implant displacement (measured at the tip) between consecutive in vivo μCT scans. Implant 1: anterior implant, implant 2: posterior implant. Black: control, blue: low force (0.5 N), orange: medium force (1.0 N), and red: high force (1.5 N)

In general, implant displacement was more pronounced in the medium and high force groups compared with the low force group (Figure 6a-d). Additionally, movement of the posterior implant was in general greater compared with the anterior implant. In the high and medium force groups, tipping occurred around a center of rotation located at about one half to one third above the implant tip. In the low force group, the center of rotation was more cervical and mostly, the implant head remained stable leading to a movement of the implant tip solely (Figure 7).

The linear mixed effects models revealed that the amount of applied force affected the movement of the anterior implant ($\chi^2$ = 12.12, *df* = 3, and *p* = .007) with an estimated between movement of 12.94 µm in the low force, 43.42 µm in the medium, and 56.56 µm in the high force groups between consecutive measurements. For the posterior implant, this relation was more pronounced ($\chi^2$ = 20.35, *df* = 3, and *p* < .001) with an estimated between measurement movement of 51.72 µm in the low force, 81.82 µm in the medium, and 84.24 µm in the high force groups.

The likelihood analyses also revealed a change of movement velocity over time. For the anterior implant, movement decreased after week one (week 1–2: −24.38 µm, week 2–4: −28.85 µm, week 4–6: −26.55, week 6–8: −32.38, $\chi^2$ = 20.35, *df* = 3, and *p* < .001). For the distal implant, a clear decrease was noted after week two (week 1–2:8.33 µm, week 2–4: −22.48 µm, week 4–6: −35.00 µm, week 6–8:34.12 µm, $\chi^2$ = 6.17, *df* = 4, and *p* = .047).

### 3.4 | Bone remodeling

Assessment of the associated bone remodeling was performed using the registered scans from different time points. Visually, an increase in cortical thickness was observed at the dorsal and interproximal portion of the vertebra in all animals. This increase was most pronounced in the medium and high force groups. In these groups, extensive bone formation was also observed in the mid-portion of the vertebra. At 8 weeks, areas of dense bone existed distal to the tip of the implants and mesial from the upper part of the implants. At the distal neck of implants with extensive tipping, newly formed bone with a woven like pattern was identified. Two animals exhibited a large circular defect after implant movement, and in three animals, a small dehiscence was noted distal from the posterior implant. Despite in most of the animals, the void at the initial position of the implant was filled with newly formed bone both at the top and at the tip of the implants.

In the low force group, bone apposition was also observed in the directions of expected compressive force, in the mid-portion and at the dorsal and interproximal aspects at 8 weeks of healing. In the control group, minor bone formation was found, and bone formation was observed circular around the implants.

## 4 | DISCUSSION

Whereas stationary stability of implants has been postulated, clinical observations revealed that implant displacement may occur under constant loading (Liou et al., 2004). Hence, the present study aimed at assessing whether orthodontic forces can induce implant movement in bone. Additionally, a linear association between applied force and velocity of implant displacement was hypothesized.

The present longitudinal data demonstrated that minor movements of implants are associated with a regular healing process. Despite forces of 1.0 N and 1.5 N induced distinct movements,

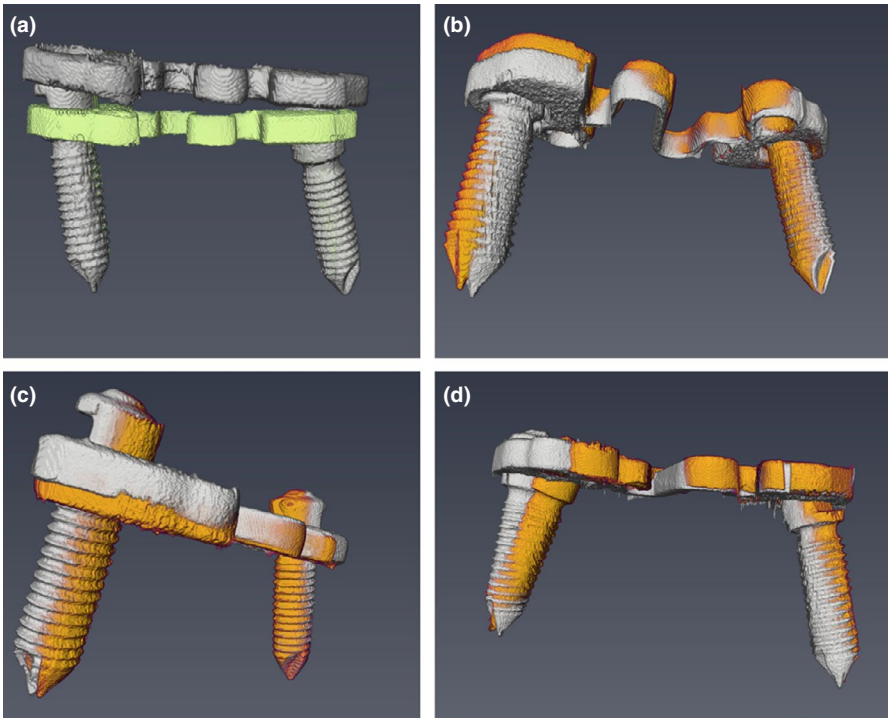


**FIGURE 7** Volumetric renderings of implant displacement between week 0 and week 8 in the (a) control group (0 N), (b) low force group (0.5 N), (c) medium force (1.0 N), and (d) high force group (1.5 N). Gray: Implants and spring after surgery, colored: implants and spring after 8 weeks

usually accompanied by new bone formation at the former implant position (Figure 8a-d). In very few cases (i.e., three animals), small defects were observed distal from the implant neck, and in further two animals, large defects were found around one of two implants. In several animals, movement existed until termination of the study. In contrast, the low force (0.5 N) group showed a minor movement of the implants and in most animals, movement decreased during the experimental phase. Additionally, a cortical thickening especially mesial to the implant neck and distal to the implant tip was observed and accompanied by a general thickening of the dorsal cortical compartment and the inner cancellous part.

From a clinical perspective, this observation is relevant because implants may no longer be regarded as fully ankylosed. Instead, they seem to interfere with the regular remodeling process occurring in bone. The linear relationship between implant displacement and applied force dictates that anatomical structures adjacent to continuously loaded implants may be affected by implant movement, for example, tooth roots may be harmed or displaced when interradicular orthodontic mini-implants are loaded. Considering that the screws employed in the present investigation were of reduced size and that orthodontic implants are by factor three larger, absolute displacements in human may be much more pronounced compared with the present investigation. Furthermore, positional changes seemed to occur without bacterial infection.

Stimulation of bone remodeling by compressive forces has been reported in numerous studies, and volumetric micro-tomographic analyses revealed increases in volume fraction and mineral content (Berman, Clauser, Wunderlin, Hammond, & Wallace, 2015; Fritton, Myers, Wright, & Meulen, 2005; Weatherholt, Fuchs, & Warden, 2013; Yang, Embry, & Main, 2017). Most recently, an increase in peri-implant bone formation following cyclic loading has been described in a longitudinal in vivo μCT study in murine vertebrae, and bone formation also correlated with the strains computed through micro-finite element method (Li et al., 2019). In this context, it has to be noted that previous studies did not apply continuous forces, and the magnitude was also much higher compared with the present investigation. The mechanobiological reaction in the compressive areas is in line with previous observations, and potentially, it also caused the decrease of implant movement over time. As implant migration occurred during the entire period of investigation in several animals, a sole association with the elastic properties of the bone appears unlikely thus pointing at local mechanobiological adaptive processes. Further investigations are needed to assess the local gene expression and potential time-dependent stimulation of macrophages, osteoclasts, and osteoblasts in the respective areas.

A particular interesting observation is that bone formation occurred at the former implant position in most animals whereas in very few rats, a small or even larger dehiscence became eminent. In this context it has to be noted that remains unclear whether the new bone formation is linked to the inflammatory process which occurs within hours after implant insertion (Bielemann, Marcello-Machado, Bel Cury, & Faot, 2018; Bosshardt et al., 2017; Insua, Monje, Wang, & Miron, 2017). As this inflammatory process provokes bone remodeling (Ma et al., 2018), the movement of the implant might have induced a distraction of the newly formed woven bone (Meyers, Schulke, Ignatius, & Claes, 2017, 2018). However, further research is needed to investigate the associated molecular patterns and also potential relationships to early implant failures.

The rat tail model has been sparsely mentioned in dental literature. It was first described by M. L. Wang, Massie, Perry, Garfin, and Kim (2007) for analyzing the impact of bone loading in osteoporotic animals. It was introduced to dentistry in 2016 by Renaud et al. (2016) and further described by Farkasdi et al. (2018). A big advantage of this animal model is the relative ease of interoperative accessibility, and, due to the small size of the tail, high-resolution μCT images can be obtained from living animals. Compared with the intraoral apparatus of rats which contains for the most part cortical bone, the vertebrae comprise a cortical and cancellous compartment. At a vertebra length of about 10 mm, two mini-implants can be placed in the same vertebra most of the time. Hence, the rat tail

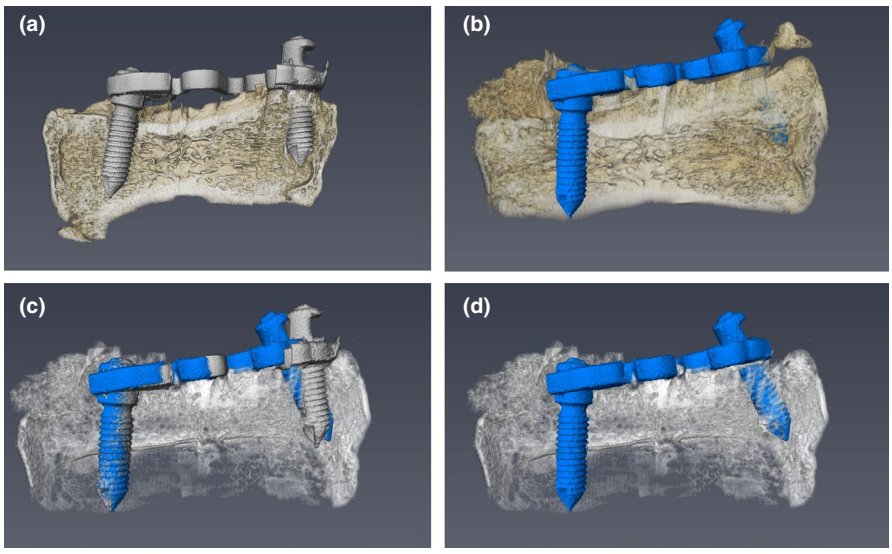


**FIGURE 8** Example of the bone remodeling and implant displacement of one specimen in the high force group. (a) Volume rendering of the situation after surgery. (b) Situation 8 weeks after surgery, (c, d) new bone formation between week one and 8. Original implant position: gray, new implant position after movement: blue

model allows to assess the dynamics of bone healing and adaptive remodeling in a longitudinal in vivo micro-computed study.

It may be questioned to what extent residual growth of the rat vertebrae had an impact on the findings of the present investigation. At the age of 15 weeks, female rats already show a very low growth rate, whereas male rats still exhibit a pronounced gain in body weight and length (Pahl, 1969; Slob & van der Werff Ten Bosch, 1975; Svingen et al., 2018). Additionally, residual growth occurs at the sutures so the vertebrae prolongate lateral from the implants. Respecting that female rats were used and that the implants were contracted, an impact of residual growth on the present findings appears unlikely. Rigid registration of the bone tissues was employed because growth was already at a very low rate. In contrast, affine registration of growing vertebrae might overestimate implant displacement as this phenomenon occured in the opposite direction.

A limitation of intravital radiography is restriction in scanning time. Especially, materials with high atomic numbers are prone to metal artefacts. Hence, prolonged scanning would be needed to average them out, but longer narcosis and radiation would also be detrimental for the animals. As a consequence, in vivo scans are usually of lower quality compared with specimen scans. In the present study, consistent orientation of the spring along the z-axis of the scanner and 40 min of scanning turned out to be required to achieve reliable segmentation of the bone and implants.

Inhibition of bone remodeling through analgesia is well documented in literature, and a direct relationship between cycloocygenase-2 inhibitors on osteoclastogenesis and bone resorption have been reported (Bonewald & Johnson, 2008; Jain et al., 2014; Kamel, Picconi, Lara-Castillo, & Johnson, 2010; Kawashima, Fujikawa, Itonaga, Takita, & Tsumura, 2009; Lara-Castillo et al., 2015). Therefore, buprenorphine, that is, a derivate of the opioid thebaine, was injected at a very lose dose for 3 days post-operatively in the present study. Whereas an impact on bone metabolism cannot be excluded, we aimed to avoid manipulation of the early healing phase through inhibition of prostaglandin-e2 synthesis.

An impact of surface roughness on the inflammatory and overall cellular response during peri-implant bone healing was noted in previous studies (Bielemann et al., 2018; Ma et al., 2018; Rupp, Liang, Geis-Gerstorfer, Scheideler, & Huttig, 2018). According to a systematic review, rough ($S_a$ > 2.0 μm) and moderate rough surfaces ($S_a$ > 1.0–2.0 μm) revealed higher bone-to-implant contact values compared with smooth ($S_a$ < 0.5 μm) and minimally rough ($S_a$ 0.5–1.0 μm) surfaces (Wennerberg & Albrektsson, 2009). In the present investigation, the implant surfaces were minimally rough, and neither polishing nor etching or sandblasting was performed to enhance surface characteristics. As shown in Figure 2, no detrimental material was visible on the surfaces. Despite it has to be noted that most dental and a few orthodontic implants are subject to surface treatment after fabrication, and hence, bone response may be different at implants with modified surfaces.

Another limitation of the present investigation is that the impact of immediate loading versus delayed loading was not investigated. Despite fully osseointegrated implants may react differently on constant forces once inflammatory cytokine levels have decreased (Bielemann et al., 2018). In the rat tail animal model, the spring has to be located subcutaneously, thus delayed loading would imply another surgical intervention and therefore a second peek of inflammatory cytokines.

In terms of translateability to human, another limitation is that neither jaw muscle function nor age-related changes have an impact on bone remodeling in rat vertebrae. In human, arch lengths and intercanine widths change with age as reported by Tsiopas, Nilner, Bondemark, and Bjerklin (2013). It should be noted that these aspects cannot be reflected in the rat tail animal model.

In conclusion and within the limitations of the present investigation, it could be demonstrated that constant forces can induce migration of implants in bone. The longitudinal μCT data suggest that this process is associated with local and distant bone remodeling, that is, load-induced apposition and resorption of bone. Additionally, a significant linear and time-dependent association between the magnitude of applied force and velocity of displacement was found. Future studies are needed to assess the associated gene expression and molecular healing patterns, as well as of the impact of immediate versus delayed loading protocols.

## ACKNOWLEDGEMENTS

The authors highly appreciate the work of Romano Matthys and Reto Nützi from RISystem AG (Landquart, Switzerland) who were involved in the development and fabrication of the customized flat nickel–titanium springs, and who also developed and fabricated the customized mini-implants. Furthermore, the authors express their gratefulness to Martin Sager, Jeanette Knorr, and Iris Schrey (ZETT) who were involved in the anesthesia and analgesia of the animals. Further gratitude is expressed to Jörg Breitkreuz and Karin Matthée (Institute of Pharmaceutics and Biopharmaceutics) who contributed the DSC analysis. Manuel Nienkemper is being thanked for his support in the conception of the study. For the programming of the robot to perform the biomechanical analyses of the springs, the authors thank Ralf Hönscheid. Markus Kraft from Altatec GmbH is given gratitude for the surface analysis of the mini-implants. Finally, the authors highly appreciate the help of Mira Hüfner, Pernille Jensen, and Viktoria Trelenberg-Stoll who were involved in the image registration and validation of the implant displacement measurements.

## CONFLICT OF INTERESTS

The authors declare that they have no conflict of interests related to this study.

## ORCID


*Kathrin Becker* https://orcid.org/0000-0003-1936-4683

*Frank Schwarz* https://orcid.org/0000-0001-5515-227X

## REFERENCES


Alves, M. Jr, Baratieri, C., & Nojima, L. I. (2011). Assessment of mini-implant displacement using cone beam computed tomography. *Clinical Oral Implants Research*, *22*(10), 1151–1156. https://doi.org/10.1111/j.1600-0501.2010.02092.x

Bates, D., Maechler, M., Bolker, B., & Walker, S. (2015). Fitting linear mixed-effects models using lme4. *Journal of Statistical Software*, *67*(1), 1–48. https://doi.org/10.18637/jss.v067.i01

Becker, K., Pliska, A., Busch, C., Wilmes, B., Wolf, M., & Drescher, D. (2018). Efficacy of orthodontic mini implants for en masse retraction in the maxilla: A systematic review and meta-analysis. *International Journal of Implant Dentistry*, *4*(1), 35. https://doi.org/10.1186/s40729-018-0144-4

Becker, K., Stauber, M., Schwarz, F., & Beissbarth, T. (2015). Automated 3D–2D registration of X-ray microcomputed tomography with histological sections for dental implants in bone using chamfer matching and simulated annealing. *Computerized Medical Imaging and Graphics*, *44*, 62–68. https://doi.org/10.1016/j.compmedimag.2015.04.005

Becker, K., Wilmes, B., Grandjean, C., Vasudavan, S., & Drescher, D. (2018). Skeletally anchored mesialization of molars using digitized casts and two surface-matching approaches: Analysis of treatment effects. *Journal of Orofacial Orthopedics / Fortschritte der Kieferorthopädie*, *79*(1), 11–18. https://doi.org/10.1007/s00056-017-0108-y

Berman, A. G., Clauser, C. A., Wunderlin, C., Hammond, M. A., & Wallace, J. M. (2015). Structural and mechanical improvements to bone are strain dependent with axial compression of the tibia in female C57BL/6 mice. *PLoS ONE*, *10*(6), e0130504. https://doi.org/10.1371/journal.pone.0130504

Bielemann, A. M., Marcello-Machado, R. M., Del Bel Cury, A. A., & Faot, F. (2018). Systematic review of wound healing biomarkers in peri-implant crevicular fluid during osseointegration. *Archives of Oral Biology*, *89*, 107–128. https://doi.org/10.1016/j.archoralbio.2018.02.013

Bonewald, L. F., & Johnson, M. L. (2008). Osteocytes, mechanosensing and Wnt signaling. *Bone*, *42*(4), 606–615. https://doi.org/10.1016/j.bone.2007.12.224

Bosshardt, D. D., Chappuis, V., & Buser, D. (2017). Osseointegration of titanium, titanium alloy and zirconia dental implants: current knowledge and open questions. *Periodontology 2000*, *73*(1), 22–40. https://doi.org/10.1111/prd.12179

Dall'Ara, E., Boudiffa, M., Taylor, C., Schug, D., Fiegle, E., Kennerley, A. J., … Müller, R. (2016). Longitudinal imaging of the ageing mouse. *Mechanisms of Ageing and Development*, *160*, 93–116. https://doi.org/10.1016/j.mad.2016.08.001

Farkasdi, S., Pammer, D., Rácz, R., Hriczó-Koperdák, G., Szabó, B. T., Dobó-Nagy, C., … Varga, G. (2018). Development of a quantitative preclinical screening model for implant osseointegration in rat tail vertebra. *Clinical Oral Investigations*, *23*(7), 2959–2973. https://doi.org/10.1007/s00784-018-2661-1

Fritton, J. C., Myers, E. R., Wright, T. M., & van der Meulen, M. C. (2005). Loading induces site-specific increases in mineral content assessed by microcomputed tomography of the mouse tibia. *Bone*, *36*(6), 1030–1038. https://doi.org/10.1016/j.bone.2005.02.013

Insua, A., Monje, A., Wang, H. L., & Miron, R. J. (2017). Basis of bone metabolism around dental implants during osseointegration and peri-implant bone loss. *Journal of Biomedical Materials Research Part A*, *105*(7), 2075–2089. https://doi.org/10.1002/jbm.a.36060

Jain, N. X., Barr-Gillespie, A. E., Clark, B. D., Kietrys, D. M., Wade, C. K., Litvin, J., … Barbe, M. F. (2014). Bone loss from high repetitive high force loading is prevented by ibuprofen treatment. *Journal of Musculoskeletal and Neuronal Interactions*, *14*(1), 78–94.

Kamel, M. A., Picconi, J. L., Lara-Castillo, N., & Johnson, M. L. (2010). Activation of β-catenin signaling in MLO-Y4 osteocytic cells versus 2T3 osteoblastic cells by fluid flow shear stress and PGE2: Implications for the study of mechanosensation in bone. *Bone*, *47*(5), 872–881. https://doi.org/10.1016/j.bone.2010.08.007

Kanomi, R. (1997). Mini-implant for orthodontic anchorage. *Journal of Clinical Orthodontics*, *31*(11), 763–767.

Kawashima, M., Fujikawa, Y., Itonaga, I., Takita, C., & Tsumura, H. (2009). The effect of selective cyclooxygenase-2 inhibitor on human osteoclast precursors to influence osteoclastogenesis in vitro. *Modern Rheumatology*, *19*(2), 192–198. https://doi.org/10.1007/s10165-008-0149-6

Kong, M. C., Axinte, D., & Voice, W. (2011). Challenges in using waterjet machining of NiTi shape memory alloys: An analysis of controlled-depth milling. *Journal of Materials Processing Technology*, *211*(6), 959–971. https://doi.org/10.1016/j.jmatprotec.2010.12.015

Lara-Castillo, N., Kim-Weroha, N. A., Kamel, M. A., Javaheri, B., Ellies, D. L., Krumlauf, R. E., … Johnson, M. L. (2015). In vivo mechanical loading rapidly activates beta-catenin signaling in osteocytes through a prostaglandin mediated mechanism. *Bone*, *76*, 58–66. https://doi.org/10.1016/j.bone.2015.03.019

Li, Z., Betts, D., Kuhn, G., Schirmer, M., Müller, R., & Ruffoni, D. (2019). Mechanical regulation of bone formation and resorption around implants in a mouse model of osteopenic bone. *Journal of the Royal Society Interface*, *16*(152), 20180667. https://doi.org/10.1098/rsif.2018.0667

Li, Z., Kuhn, G., von Salis-Soglio, M., Cooke, S. J., Schirmer, M., Muller, R., & Ruffoni, D. (2015). In vivo monitoring of bone architecture and remodeling after implant insertion: The different responses of cortical and trabecular bone. *Bone*, *81*, 468–477. https://doi.org/10.1016/j.bone.2015.08.017

Liou, E. J., Pai, B. C., & Lin, J. C. (2004). Do miniscrews remain stationary under orthodontic forces? *American Journal of Orthodontics and Dentofacial Orthopedics*, *126*(1), 42–47. https://doi.org/10.1016/s0889540604002057

Ma, Q. L., Fang, L., Jiang, N., Zhang, L., Wang, Y., Zhang, Y. M., & Chen, L. H. (2018). Bone mesenchymal stem cell secretion of sRANKL/OPG/M-CSF in response to macrophage-mediated inflammatory response influences osteogenesis on nanostructured Ti surfaces. *Biomaterials*, *154*, 234–247. https://doi.org/10.1016/j.biomaterials.2017.11.003

Melsen, B., & Costa, A. (2000). Immediate loading of implants used for orthodontic anchorage. *Clinical Orthodontics and Research*, *3*(1), 23–28. https://doi.org/10.1034/j.1600-0544.2000.030105.x

Meyers, N., Schulke, J., Ignatius, A., & Claes, L. (2017). Novel systems for the application of isolated tensile, compressive, and shearing stimulation of distraction callus tissue. *PLoS ONE*, *12*(12), e0189432. https://doi.org/10.1371/journal.pone.0189432

Meyers, N., Schulke, J., Ignatius, A., & Claes, L. (2018). Evolution of callus tissue behavior during stable distraction osteogenesis. *Journal of the Mechanical Behavior of Biomedical Materials*, *85*, 12–19. https://doi.org/10.1016/j.jmbbm.2018.05.017

Meyns, J., Brasil, D. M., Mazzi-Chaves, J. F., Politis, C., & Jacobs, R. (2018). The clinical outcome of skeletal anchorage in interceptive treatment (in growing patients) for class III malocclusion. *International Journal of Oral and Maxillofacial Surgery*, *47*(8), 1003–1010. https://doi.org/10.1016/j.ijom.2018.04.011

Nienkemper, M., Handschel, J., & Drescher, D. (2014). Systematic review of mini-implant displacement under orthodontic loading. *International Journal of Oral Science*, *6*(1), 1–6. https://doi.org/10.1038/ijos.2013.92

Pahl, P. J. (1969). Growth curves for body weight of the laboratory rat. *Australian Journal of Biological Sciences*, *22*(4), 1077–1080. https://doi.org/10.1071/BI9691077

Papageorgiou, S. N., Zogakis, I. P., & Papadopoulos, M. A. (2012). Failure rates and associated risk factors of orthodontic miniscrew implants: A meta-analysis. *American Journal of Orthodontics and Dentofacial Orthopedics*, *142*(5), 577.e7–595.e7. https://doi.org/10.1016/j.ajodo.2012.05.016

Park, H. S., Bae, S. M., Kyung, H. M., & Sung, J. H. (2001). Micro-implant anchorage for treatment of skeletal Class I bialveolar protrusion. *J Clin Orthod*, *35*(7), 417–422.

R Core Team (2016). *R: A language and environment for statistical computing*. Vienna, Austria: R Foundation for Statistical Computing. https://www.R-project.org/

Renaud, M., Farkasdi, S., Pons, C., Panayotov, I., Collart-Dutilleul, P.-Y., Taillades, H., … Yachouh, J. (2016). A new rat model for translational research in bone regeneration. *Tissue Engineering Part C Methods*, *22*(2), 125–131. https://doi.org/10.1089/ten.TEC.2015.0187

Reynders, R., Ronchi, L., & Bipat, S. (2009). Mini-implants in orthodontics: A systematic review of the literature. *American Journal of Orthodontics and Dentofacial Orthopedics*, *135*(5), 564.e1–564.e19. https://doi.org/10.1016/j.ajodo.2008.09.026

Rodríguez de Guzmán-Barrera, J., Sáez Martínez, C., Boronat-Catalá, M., Montiel-Company, J. M., Paredes-Gallardo, V., Gandía-Franco, J. L., … Bellot-Arcís, C. (2017). Effectiveness of interceptive treatment of class III malocclusions with skeletal anchorage: A systematic review and meta-analysis. *PLoS ONE*, *12*(3), e0173875. https://doi.org/10.1371/journal.pone.0173875

Rupp, F., Liang, L., Geis-Gerstorfer, J., Scheideler, L., & Huttig, F. (2018). Surface characteristics of dental implants: A review. *Dental Materials*, *34*(1), 40–57. https://doi.org/10.1016/j.dental.2017.09.007

Slob, A. K., & van der Werff Ten Bosch, J. J. (1975). Sex differences in body growth in the rat. *Physiology and Behavior*, *14*(3), 353–361. https://doi.org/10.1016/0031-9384(75)90044-X

Studholme, C., Hill, D. L. G., & Hawkes, D. J. (1999). An overlap invariant entropy measure of 3D medical image alignment. *Pattern Recognition*, *32*(1), 71–86. https://doi.org/10.1016/S0031-3203(98)00091-0

Svingen, T., Ramhøj, L., Mandrup, K., Christiansen, S., Axelstad, M., Vinggaard, A. M., & Hass, U. (2018). Effects on metabolic parameters in young rats born with low birth weight after exposure to a mixture of pesticides. *Scientific Reports*, *8*(1), 305. https://doi.org/10.1038/s41598-017-18626-x

Tsiopas, N., Nilner, M., Bondemark, L., & Bjerklin, K. (2013). A 40 years follow-up of dental arch dimensions and incisor irregularity in adults. *European Journal of Orthodontics*, *35*(2), 230–235. https://doi.org/10.1093/ejo/cjr121

Wang, M. L., Massie, J., Perry, A., Garfin, S. R., & Kim, C. W. (2007). A rat osteoporotic spine model for the evaluation of bioresorbable bone cements. *The Spine Journal*, *7*(4), 466–474. https://doi.org/10.1016/j.spinee.2006.06.400

Wang, Y. C., & Liou, E. J. W. (2008). Comparison of the loading behavior of self-drilling and predrilled miniscrews throughout orthodontic loading. *American Journal of Orthodontics and Dentofacial Orthopedics*, *133*(1), 38–43. https://doi.org/10.1016/j.ajodo.2006.01.042

Weatherholt, A. M., Fuchs, R. K., & Warden, S. J. (2013). Cortical and trabecular bone adaptation to incremental load magnitudes using the mouse tibial axial compression loading model. *Bone*, *52*(1), 372–379. https://doi.org/10.1016/j.bone.2012.10.026

Wehrbein, H., Glatzmaier, J., Mundwiller, U., & Diedrich, P. (1996). The Orthosystem–a new implant system for orthodontic anchorage in the palate. *Journal of Orofacial Orthopedics*, *57*(3), 142–153.

Wehrbein, H., Merz, B. R., Diedrich, P., & Glatzmaier, J. (1996). The use of palatal implants for orthodontic anchorage. Design and clinical application of the orthosystem. *Clinical Oral Implants Research*, *7*(4), 410–416. https://doi.org/10.1034/j.1600-0501.1996.070416.x

Wennerberg, A., & Albrektsson, T. (2009). Effects of titanium surface topography on bone integration: A systematic review. *Clinical Oral Implants Research*, *20*(s4), 172–184. https://doi.org/10.1111/j.1600-0501.2009.01775.x

Wilmes, B., Katyal, V., & Drescher, D. (2014). Mini-implant-borne Pendulum B appliance for maxillary molar distalisation: Design and clinical procedure. *Australian Orthodontic Journal*, *30*(2), 230–239.

Yang, H., Embry, R. E., & Main, R. P. (2017). Effects of loading duration and short rest insertion on cancellous and cortical bone adaptation in the mouse tibia. *PLoS ONE*, *12*(1), e0169519. https://doi.org/10.1371/journal.pone.0169519

Zhou, J., Yang, F., Xu, X., Feng, G., Chen, J., Song, J., & Dai, H. (2018). Dynamic evaluation of orthodontically-induced tooth movement, root resorption, and alveolar bone remodeling in rats by in vivo micro-computed tomography. *Medical Science Monitor*, *24*, 8306–8314. https://doi.org/10.12659/msm.912470

**How to cite this article:** Becker K, Schwarz F, Rauch NJ, Khalaph S, Mihatovic I, Drescher D. Can implants move in bone? A longitudinal in vivo micro-CT analysis of implants under constant forces in rat vertebrae. *Clin Oral Impl Res*. 2019;30:1179–1189. https://doi.org/10.1111/clr.13531